Published in "The Journal of Physical Chemistry C 114(15): 7173-7177 , 2010"
which should be cited to refer to this work.

Stability and Decomposition of $NaBH_4$

Pascal Martelli,*,†,‡ Riccarda Caputo,*,† Arndt Remhof,† Philippe Mauron,† Andreas Borgschulte,† and Andreas Züttel†,‡

Division of Hydrogen & Energy, Department of Mobility, Energy and Environment, EMPA, Swiss Federal Laboratories for Materials Testing and Research, 8600 Dübendorf, and Physics Department, University of Fribourg, 1700 Fribourg, Switzerland

We investigate the stability and hydrogen desorption of $NaBH_4$. Dynamic pcT (pressure, concentration, and temperature) measurements under constant hydrogen flows are used to determine thermodynamic parameters of reaction. From the van't Hoff equation the enthalpy and entropy of reaction, -108 ± 3 kJ mol^{-1} of H_2 and 133 ± 3 J K^{-1} mol^{-1} of H_2 released, are obtained, respectively. This corresponds to a decomposition temperature of $T_{dec} = 534 \pm 10$ °C at 1 bar of H_2. The decomposition thereby occurs in one step; i.e., only one plateau is visible in the pressure composition isotherms. Elemental Na is identified as the major solid component in the residue by X-ray diffraction. The experimental results are discussed on the basis of theoretical calculations using the density functional theory approach. Starting from the optimized structure of the cubic α-phase of $NaBH_4$, we discuss possible decomposition routes involving elemental Na and B as well as Na−H and Na−B binary compounds as residual products.

Introduction

Sodium tetrahydroborate ($NaBH_4$), shortly called sodium borohydride, is widely used as a reducing agent in industrial and laboratory applications. Due to its large volumetric (115 kg of H_2 m^{-3}) and gravimetric (10.7 mass %)[1,2] hydrogen content, $NaBH_4$ has a high potential to be used as a synthetic fuel either in a direct borohydride fuel cell[3] or as a hydrogen storage material for mobile applications.[4–9] Apart from a large hydrogen content, the required properties of a technically applicable hydrogen storage material are fast sorption kinetics and convenient working temperatures and working pressures. The apparent desorption temperature, i.e., the temperature at which hydrogen is released from a compound, depends on the experimental conditions, especially on the applied pressure and heating rate. Up to now, the use of $NaBH_4$ and its chemical relatives, e.g., $LiBH_4$, $Mg(BH_4)_2$, and $Ca(BH_4)_2$, have been hindered by their high stability, leading to desorption temperatures well above room temperature. Desorption temperatures for $NaBH_4$ reported in the literature range from 400 to 595 °C.[8,10–13] These discrepancies often resulted from different experimental procedures that did not allow separation of thermodynamic from kinetic effects. Furthermore, the desorption reaction is not known in detail so far. In comparison, $LiBH_4$,[14] $Ca(BH_4)_2$,[15] and $Mg(BH_4)_2$[16] are believed to decompose via the respective metal hydrides in a two-step reaction. In principle, different decomposition paths are thermodynamically possible, which involve desorption products other than metal hydrides and amorphous boron, as, for example, investigated for $LiBH_4$.[17] On the other hand, the relatively low stability of NaH, leading to thermal decomposition above 425 °C,[11] would favor a one-step decomposition of $NaBH_4$. Nevertheless, a clear understanding of the decomposition mechanism of $NaBH_4$ and determination of thermodynamic functions are not yet fully achieved. In the present paper we report a combined experimental and theoretical study on the stability and decomposition of $NaBH_4$. We determined the thermodynamic parameters by pressure−concentration isotherms (pcT) based on a mass flow method as described elsewhere.[14,18] The desorption products were identified by X-ray diffraction. Possible paths of decomposition reaction were investigated by means of first-principles calculations, based on the density functional theory (DFT) method as already proposed for thermal decomposition of $LiBH_4$.[17]

Methods

Two different sets of experiments are carried out to investigate the thermal decomposition of $NaBH_4$. First, in a series of pcT measurements, the desorption plateaus are determined and thermodynamic parameters are obtained. Subsequently, the desorption products are identified by X-ray diffraction. The enthalpy $\Delta_r H$ and entropy $\Delta_r S$ of the desorption reaction are determined from the plateau pressure of the desorption isotherms. To obtain the equilibrium data and to exclude kinetic effects, dynamic pcT measurements are performed at different flow rates for each temperature. By this method equilibrium data are extracted by extrapolation to zero flow.[18] The logarithm of the equilibrium pressure p_{eq} divided by the standard pressure p_0 as a function of the inverse temperature is represented in a van't Hoff equation:

$$R \ln\left(\frac{p_{eq}}{p_0}\right) = \frac{\Delta_r H}{T} + \Delta_r S \qquad (1)$$

Recently, this method was successfully used to study the decomposition of $LiBH_4$.[14] The solid-state residues are identified by combining pcT measurements by postmortem X-ray diffraction of the desorbed material. Thermodynamic results as well as structural data are discussed on the basis of ab initio calculations. Pure $NaBH_4$ (Sigma-Aldrich, purity 99.99%, metals basis) is used to exclude any influence from additives or

* To whom correspondence should be addressed. E-mail: Pascal.Martelli@empa.ch (P.M.); Riccarda.Caputo@empa.ch (R.C.).
† EMPA.
‡ University of Fribourg.

TABLE 1: Calculated Thermodynamic Data and Lattice Parameters of the Species Reported in the Present Work

species	$\Delta_f H$/kJmol^{-1}	a, b, c/Å	symmetry group (IT)	remarks
$NaBH_4$	−245.500	6.199	$F\bar{4}3m$ (216)	face-centered cubic
Na	0.0	4.214	$Im\bar{3}m$ (229)	body-centered cubic[21]
α-B	0.0	4.860, 4.860, 12.414	$R\bar{3}m$ (166)	hexagonal[25]
NaH	−45.519	4.867	$Fm\bar{3}m$ (225)	face-centered cubic[23]
Na_2B_{29}	−105.213	10.240, 8.230, 5.755	$Im2m$ (44)	body-centered orthorhombic[39]
Na_2B_{30}	−281.157	10.186, 8.339, 5.777	$Imam$ (74)	body-centered orthorhombic[38]
Na_3B_{20}	−200.718	18.492, 5.623, 4.106	$Cmmm$ (65)	centered orthorhombic[37]

catalysts. The sample is solely handled in inert gas conditions or under controlled hydrogen pressure.

Pressure−Composition Isotherms (pcT). Dynamic pcT measurements are carried out in desorption by releasing hydrogen gas out of the system via a mass flow controller while monitoring the pressure. Measurements are performed over time under a constant flow of 2, 1, and 0.5 cm^3 (STP) min^{-1}. The integrated flow yields the total hydrogen volume, consisting of the amount of hydrogen desorbed from the sample and the hydrogen filling the system volume at standard conditions, i.e., the "dead volume". Subsequently, the volume, corrected for the dead volume, is converted into the respective hydrogen mass. Finally, the pressure is plotted as a function of the desorbed amount of hydrogen (mass %). For pcT measurements, 250 mg of $NaBH_4$ is filled in a stainless steel autoclave, which is airtightly closed and transferred to the pcT apparatus. Prior to measurement the sample is evacuated at room temperature to a vacuum of better than 5×10^{-3} mbar. A starting hydrogen pressure of 20 bar (purity 99.999%) is applied to the autoclave, and the sample is heated to the desired temperature (600, 650, and 700 °C). The pressure range of 20 bar is chosen to use the full range of the flow meter, and the temperature range is adjusted to the according plateau conditions. $NaBH_4$ contains 2 mol of H_2 per formula unit, corresponding to 1.54 cm^3 (STP) of hydrogen/mg of $NaBH_4$. Therefore, we expect a total hydrogen volume of 385 cm^3 (STP) to be desorbed. With an initial pressure of 20 bar and a pcT system volume of 33 cm^3, i.e., 660 cm^3 (STP), a desorption experiment lasts about 16 h for a flow of 1 cm^3 (STP) min^{-1}.

X-ray Diffraction (XRD). XRD is carried out to confirm the purity of the initial material and to identify the residue of decomposition. Representative samples are measured in glass capillaries (diameter 1 mm, wall thickness 0.01 mm), sealed under an inert argon atmosphere. The X-ray diffraction patterns presented in this work are measured using a Bruker D8 diffractometer, equipped with a Goebel mirror, selecting Cu Kα radiation with a wavelength of $\lambda = 1.5418$ Å (weighted average of Cu $K\alpha_1$ and Cu $K\alpha_2$ radiation). XRD patterns are analyzed by quantitative phase analysis using either the known structural data for $NaBH_4$,[19] Na,[20,21] and NaH[22,23] or first-principles optimized structures, as reported in Table 1.

Computational Methods. We used DFT-based methods, in particular CASTEP,[24] as implemented in Materials Studio 4.4 to optimize ion positions and lattice parameters of α-boron,[25] sodium (bcc), and all structures reported in the present work. Norm-conserving pseudopotentials are used for all atoms together with a fine mesh of k points, with an energy conversion threshold of 0.01 meV/atom, a maximum displacement of 0.001 Å, and a maximum force of 0.03 eV/Å, yielding high accuracy for energy and atomic displacements. We use Perdew−Burke−Ernzerhof 96 and the generalized gradient form (GGA-PBE) for the exchange-correlation function. The fully optimized structures calculated by CASTEP are also used as the input geometry for accurate phonon calculations using Plane-Wave Self-Consistent Field (PWscf), which is a computer code for electronic-structure calculations within density functional theory and density functional perturbation theory, using pseudopotentials and a plane-wave basis set.[26] Full geometry optimization is run for all investigated structures, and both internal atomic coordinates and lattice parameters are relaxed. The phonon calculations are performed by using CASTEP Linear Response (DFPT), as implemented in the CASTEP code.[27]

Results

Stability and Heat of Formation. Different structures of $NaBH_4$ have been reported in the literature since very early when the complex borohydrides were synthesized and studied for the first time.[19,28–32] $NaBH_4$ crystallizes in three different polymorphs. At ambient conditions (STP), the cubic α-phase is the most stable phase. The β-phase exists at low temperature, while the γ-phase is only observed at high pressure.[33]

Geometry optimization of the α-phase resulted in a face-centered structure, symmetry group $F\bar{4}3m$ (IT 216) and lattice parameter $a = 6.20$ Å, which is in agreement with the literature value.[30] Figure 1 shows the optimized structure, with the bidentate−tridentate coordination of the metal atom, typical of the alkali- and earth-alkaline-metal borohydrides.[34] Thermodynamic stability is ascertained by calculating the enthalpy of formation and performing the phonon analysis. The enthalpy of formation ($\Delta_f H(0)$) is −245.50 kJ mol^{-1} of $NaBH_4$ formed at $T = 0$ K, a value that becomes −210.73 kJ mol^{-1} by including the zero-point energy contribution of Na, α-B, H_2, and $NaBH_4$. It is worth noting that the cubic phase is not found to be the ground-state structure in our systematic study of first-principles structure determination. Therefore, we focus on the room temperature structure to have a direct comparison with the experimental compound. The heat of formation is calculated as the difference between the total electronic energy of $NaBH_4$ and the pure phase of Na(bcc), β-B(rhombohedral),[25] and hydrogen gas, according to the following reaction:

$$\mathrm{Na(s)^{bcc}} + \alpha\text{-}\mathrm{B(s)^{rh}} + 2\mathrm{H_2(g)} \rightarrow \mathrm{NaBH_4(s)^{cub}} \qquad (2)$$

All reported structures are fully optimized, and the lattice stability is checked via phonon calculations. The value of the enthalpy of formation reported in the literature ranges from −191 kJ mol^{-1} [30,35] to −188 kJ mol^{-1} [13] at $T = 300$ K, the last value being referred to the reaction between BH_3 and NaH to form $NaBH_4$, not to the synthesis from the respective elements. Table 1 summarizes the structural parameters calculated via the first-principles approach of cubic $NaBH_4$. We checked the lattice stability of the optimized structure and found that all frequencies of normal modes of vibration are positive.

Thermal Decomposition. Pressure concentration isotherms in the temperature range from 600 to 700 °C are measured during the desorption for three different hydrogen flows (2, 1, and 0.5 cm^3 (STP) min^{-1}). Each isotherm displays a single plateau, indicative of a one-step reaction (see Figure 2). For a

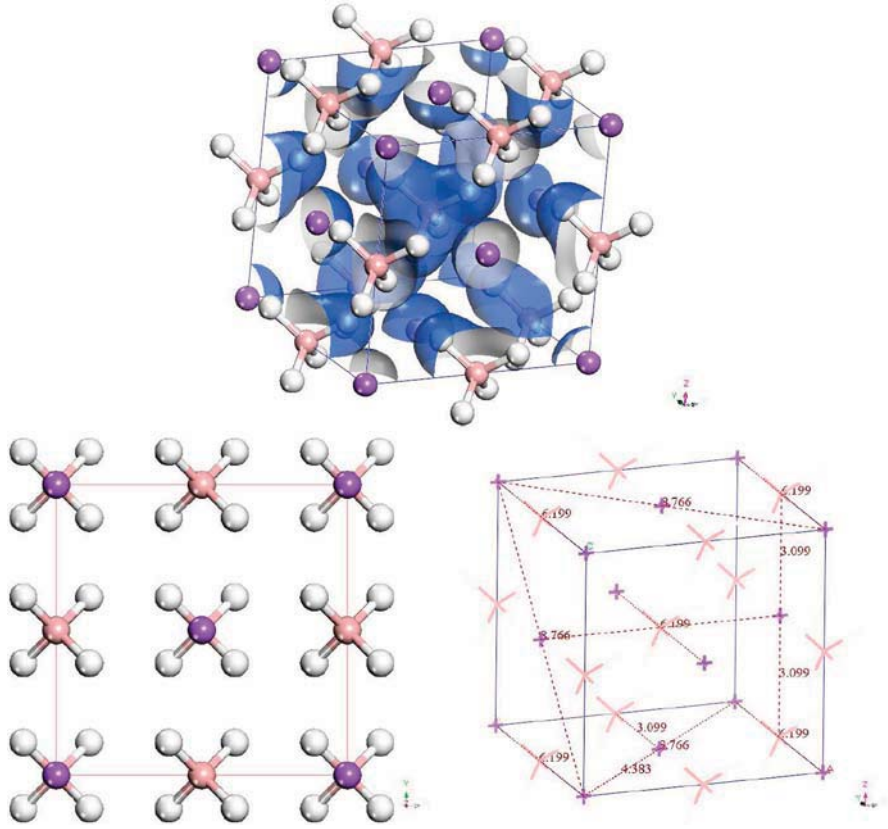

Figure 1. (Top) Crystal structure of α-$NaBH_4$ with symmetry group $F\bar{4}3m$ and lattice parameter $a = 6.199$ Å. The isodensity surface at 0.20 electron $Å^{-3}$ of the total electron density is reported to show the ionic character. Purple, pink, and white spheres represent Na, B, and H atoms, respectively. (bottom left) Top view along the [00$\bar{1}$] direction. (Left) The sodium atoms form an fcc sublattice with lattice parameter $a' = 6.199$ Å on the octahedral sides of which (four sites per unit cell) reside the $[BH_4]$ groups molecularly oriented to have the lowest energy coordination of the sodium atoms, which is the tridentate−bidentate one.

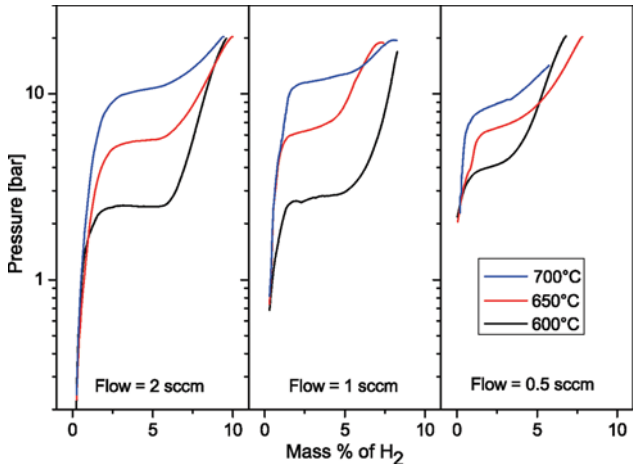

Figure 2. pcT isotherms measured at a constant hydrogen flow of 2 (a), 1 (b), and 0.5 (c) cm^3 (STP) min^{-1}.

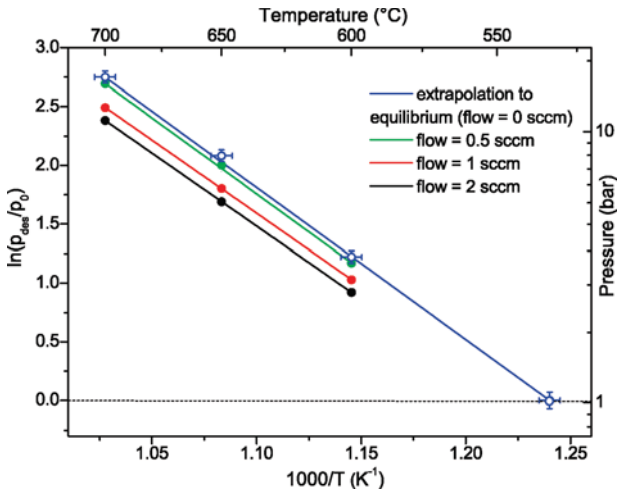

Figure 3. Van't Hoff plot of the plateau pressures for the desorption of $NaBH_4$. $\ln(p_{eq}/p_0)$ is plotted as a function of the inverse temperature $1/T$. Note that the slope and the intercept give $-\Delta H$ and ΔS of the decomposition. The filled symbols are the measurements, and the open symbols are the extrapolation to equilibrium. The cross bars reflect the error bars.

flow of 2 cm^3 (STP) min^{-1} the desorbed amount of hydrogen is 10 ± 1 mass %, and for flows of 1 and 0.5 cm^3 (STP) min^{-1} it is 8 ± 1 mass %. As the hydrogen content of $NaBH_4$ is 10.66 mass %, an observed desorption of 10 ± 1 mass % leads to the conclusion that the desorption is completed at this point and that no further plateau is expected at lower pressures. For each temperature, a single plateau is observed. The plateau pressure p_{des} for each desorption isotherm is taken in the middle of each plateau. For a given temperature the plateau pressure depends on the applied hydrogen flow and decreases with an increasing flow, indicating that the kinetics of the material is slow. If $\ln(p_{des}/p_0)$ is plotted as a function of the hydrogen flow, a straight line can be fitted to the measured points and the plateau pressure is extrapolated to the equilibrium pressure p_{eq} located at a zero flow.[14,18] Extrapolation results are shown in Figure 3, in which filled symbols correspond to the measured plateau pressures and open symbols to the extrapolated equilibrium pressures p_{eq}. The extrapolated values lie on a straight line. Applying the van't Hoff equation to the data, the following values for the enthalpy and entropy of reaction are found: $\Delta_r H = -108 \pm 3$ kJ mol^{-1}

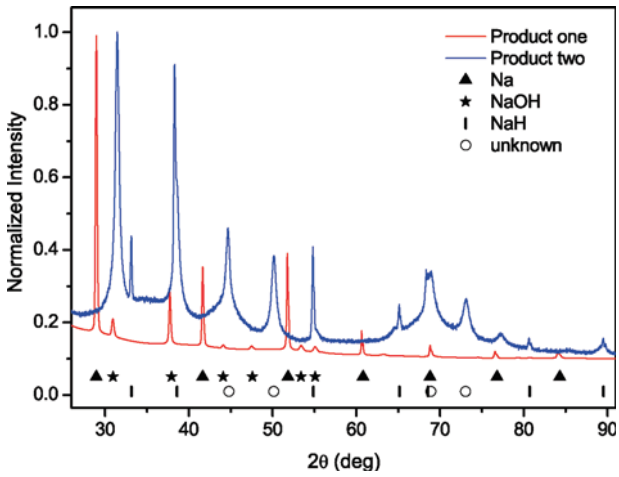

Figure 4. X-ray diffraction pattern of the two products after desorption. The filled symbols represent the detected peaks and the empty symbols the unknown peaks.

of H_2 and $\Delta_r S = 133 \pm 3$ J K^{-1} mol^{-1} of H_2, respectively. These values permit the deduction of the decomposition temperature for $NaBH_4$, $T_{dec} = \Delta H/\Delta S \Rightarrow T_{dec} = 534 \pm 10$ °C, as can be seen in Figure 3. Our result thereby is close to the value of 565 °C reported by Sterlyadkina.[36]

The desorbed product consists of two distinct solid phases: a lump of a soft, gray metallic material and a black powder. Both phases are already separated at the end of the desorption experiment. The weight ratio of both phases of about 2:1 is equal to the ratio of the atomic weights of Na to B. Both materials are investigated independently by means of XRD. The resulting diffractograms are shown in Figure 4. For easier comparability, both diffraction patterns are normalized to the strongest reflection. As the metallic material is too ductile to be ground and filled into a capillary, it is placed on a flat sample holder and covered with a transparent, semispherical X-ray window to minimize exposure to ambient air. The main diffraction peaks of the first product are identified as reflections from metallic Na, marked by triangular symbols in the figure. NaOH (marked by stars) is identified as the major impurity. As there was no oxygen in the initial compound, we attribute the occurrence of NaOH to superficial corrosion of the highly reactive metal during the transfer to the diffractometer. In the case of the second phase, the black powder, the situation is less clear. Compared to the first one, the diffraction pattern is characterized by broader reflections and by a more pronounced background, indicative of less order and the presence of one or more amorphous phases. The most intense peaks at 30.5°, 37.6°, and 43.7° are identified as NaOH, while the rather sharp reflections at 32.7°, 37.9°, 54.3°, and at 64.6° originate from NaH (marked by vertical sticks). Reflections at 44.7°, 50.1°, 66.8°, and 73.0° could not be identified (marked by open circles).

Discussion

In a very general way, the thermal decomposition follows:

$$NaBH_4 \rightarrow \sum_i \text{solid}_i(\text{Na, B, H}) + \sum_j \text{gas}_j(\text{B, H}) \quad (3)$$

where the solid residue can be formed by elemental Na and B, by binary phases, e.g., Na−B or Na−H, or by a ternary phase, Na−B−H. Elemental Na is identified as the major component

TABLE 2: Enthalpy of Reactions of Some of the Possible Decomposition Paths of $NaBH_4$, According to the Following General Reaction: $NaBH_4(s) \rightarrow \sum_i \text{solid}_i(\text{Na, B}) + H_2$[a]

reactant	solid-phase products					gas-phase		
$NaBH_4$	Na	B	NaH	Na_2B_{30}	Na_3B_{20}	product H_2	η	$\Delta_r H(0)$
1	1	1				2	2	+245.500
2		2	2			3	1.500	+199.981
30	28			1		60	2.000	+236.128
20	17				1	40	2.000	+235.464
30			28	1		46	1.533	+193.643
40			34		2	63	1.575	+196.773

[a] The enthalpy of reaction is expressed in kilojoules per mole of $NaBH_4$ decomposed. The hydrogen yield (η) is the molar ratio between the moles of hydrogen released and moles of $NaBH_4$ decomposed. The phases considered for each species were cubic $NaBH_4$, bcc Na, α-rhombohedral boron,[25] and the boron-rich binary phases reported in Table 1. In regard to H_2, the structure was optimized as an isolated molecule in a large cubic lattice.

in the solid residue. The weight ratio of about 2:1 of the two solid phases in the residue matches the weight ratio of Na and B present in the initial $NaBH_4$. Therefore, we deduce that the second phase is elemental boron or a boron-rich phase. Accordingly, we restrict our theoretical calculations to the elements Na and B and to the formation of boron-rich binary Na−B phases. We found three stable binary phases with Na:B atomic ratios of 2:29, 2:30, and 3:20. Those compounds are fully optimized as to the atomic positions and the lattice parameters, and the corresponding symmetry is compared with that of reported structures.[37–39] Table 1 lists the corresponding structural and thermodynamic data. Table 2 compares possible paths of decomposition, which lead to the formation of elemental sodium, sodium hydride, and boron-rich binary Na−B phases as solid phases and pure H_2 as the only gaseous phase. The corresponding enthalpies of reaction fall in the range of 200 kJ mol^{-1} of $NaBH_4$. The enthalpy of reaction is calculated as the difference of the enthalpy of formation between the products and reagent, each with appropriate stoichiometric coefficients and a fully optimized geometry. Thermodynamically, the decomposition path leading to the formation of elemental Na is competitive with the commonly reported path, namely, the decomposition in sodium hydride and elemental boron.

Experimentally, we cannot distinguish between these cases. The high stability of $NaBH_4$ leads to a desorption temperature which is above the desorption temperature of NaH. In other words, the equilibrium pressure for the reaction $2Na + H_2 \leftrightarrow 2NaH$ lies above the observed plateau pressures for the decomposition of $NaBH_4$, as displayed in Figure 2. Therefore, NaH is thermodynamically unstable under the decomposition condition of $NaBH_4$ and will decompose into the elements without changing the observed equilibrium pressure. Thus, experimentally, we will observe elemental Na in the residue, whether the decomposition involves NaH as an intermediate or not. The Na:NaH ratio in the residue is determined by the reaction kinetics involved. The presence of traces of NaH in the residue shows that $NaBH_4$ decays at least partially via NaH.

Conclusions

We investigated the thermal hydrogen desorption of $NaBH_4$. The stability of $NaBH_4$ is determined from pressure−composition isotherms. The dynamic measurements are carried out at constant hydrogen flows of 2, 1, and 0.5 cm^3 min^{-1}. The decomposition occurs in one step; i.e., only one plateau is visible in the isotherms. The equilibrium pressures extrapolated to zero

flow are used to determine the thermodynamic parameters. From the van't Hoff equation we have calculated $\Delta H = -108$ kJ mol^{-1} of H_2 and $\Delta S = 133$ J K^{-1} mol^{-1} of H_2. This corresponds to a decomposition temperature of $T_{dec} = 534 \pm 10$ °C at 1 bar of H_2. Elemental Na is identified as the major solid component in the residue by X-ray diffraction. These experimentally obtained thermodynamic values are compared to calculated values of ΔH and ΔS of various possible decomposition reactions using the density functional theory approach. Thereby, we focused on those reactions that yield NaH or metallic Na and H_2 in the residue (Table 2). The calculated decomposition paths involving sodium borides such as Na_2B_{30} possess reaction enthalpies of about 200 kJ mol^{-1} of $NaBH_4$ similar to that of the decomposition path leading to sodium hydride and elemental boron.

The thermal decomposition of $NaBH_4$ thereby differs markedly from that of it is chemical relative $LiBH_4$. The reason lies in the lower stability of NaH ($\Delta H = -113$ kJ mol^{-1} of H_2) as compared to LiH ($\Delta H = -233$ kJ mol^{-1} of H_2).

Acknowledgment. Financial support by the Swiss National Science Foundation (Schweizerischer Nationalfonds, SNF), Project Nos. 200020-115875 and 200021-119972/1, is gratefully acknowledged. R.C. gratefully acknowledges financial support from the European Commission DG Research RTN Marie Curie Actions-Hydrogen (Contract MRTN-CT-2006-032474, until February 2009) and the 7.Serie Interner F+E-Projekte, EMPA funding. The computer facilities IPAZIA at EMPA in Dübendorf, Switzerland, are highly appreciated.

References and Notes

(1) *CRC Handbook of Chemistry and Physics*; CRC Press: Boca Raton, FL, 2005.
(2) Schlapbach, L.; Züttel, A. *Nature* **2001**, *414*, 353–358.
(3) Liu, B. H.; Li, Z. P. *J. Power Sources* **2009**, *187*, 291–297.
(4) Züttel, A.; Borgschulte, A.; Schlapbach, L. *Hydrogen as a Future Energy Carrier*; Wiley-VCH: New York, 2008.
(5) Züttel, A. *Naturwissenschaften* **2004**, *91*, 157–172.
(6) Züttel, A.; Borgschulte, A.; Orimo, S. *Scr. Mater.* **2007**, *56*, 823–828.
(7) Orimo, S.; Nakamori, Y.; Eliseo, J. R.; Züttel, A.; Jensen, C. M. *Chem. Rev.* **2007**, *107*, 4111–4132.
(8) Felderhoff, M.; Weidenthaler, C.; von Helmolt, R.; Eberle, U. *Phys. Chem. Chem. Phys.* **2007**, *9*, 2643–2653.
(9) Crabtree, G. W.; Dresselhaus, M. S.; Buchanan, M. V. *Phys. Today* **2004**, 39–44.
(10) Schlesinger, H. I.; Brown, H. C.; Hoekstra, H. R.; Rap, L. R. *J. Am. Chem. Soc.* **1952**, *75*, 199–204.
(11) Grochala, W.; Edwards, P. *Chem. Rev.* **2004**, *104*, 1283–1315.
(12) Fedevna, E.; Alpatova, V.; Mikheeva, V. *Russ. J. Inorg. Chem.* **1964**, *9*, 826–827.
(13) Urgnani, J.; Torres, F.; Palumbo, M.; Baricco, M. *Int. J. Hydrogen Energy* **2008**, *33*, 3111–3115.
(14) Mauron, P.; Buchter, F.; Friedrichs, O.; Remhof, A.; Bielmann, M.; Zwicky, C. N.; Züttel, A. *J. Phys. Chem. B* **2008**, *112*, 906–910.
(15) Buchter, F.; Łodziana, Z.; Remhof, A.; Friedrichs, O.; Borgschulte, A.; Mauron, P.; Züttel, A.; Sheptyakov, D.; Barkhordarian, G.; Bormann, R.; Chłopek, K.; Fichtner, M.; Sørby, M.; Riktor, M.; Hauback, B.; Orimo, S. *J. Phys. Chem. B* **2008**, *112*, 8042–8048.
(16) Matsunaga, T.; Buchter, F.; Mauron, P.; Bielman, A.; Nakamori, Y.; Orimo, S.; Ohba, N.; Miwa, K.; Towata, S.; Züttel, A. *J. Alloys Compd.* **2008**, *459*, 583–588.
(17) Caputo, R.; Züttel, A. *Mol. Phys.*, in press.
(18) Bielmann, M.; Kato, S.; Mauron, P.; Borgschulte, A.; Züttel, A. *Rev. Sci. Instrum.* **2009**, *80*, 083901.
(19) Fischer, P.; Züttel, A. *Mater. Sci. Forum* **2004**, *443−444*, 287–290.
(20) Berliner, R.; Fajen, O.; Smith, H. G.; Hitterman, R. *Phys. Rev. B* **1989**, *40*, 12086–12097.
(21) Hull, A. *Phys. Rev.* **1917**, *10*, 661–696.
(22) Shull, C.; Wollan, E.; Morton, G.; Davidson, W. *Phys. Rev.* **1948**, *73*, 842–847.
(23) Zintl, E.; Harder, A. *Z. Phys. Chem., Abt. B* **1931**, *14*, 265–284.
(24) Clark, S.; Segall, M.; Pickard, C.; Haspin, P.; Probert, M.; Refson, K.; Payne, M. *Z. Krystallogr.* **2005**, *220*, 567.
(25) Caputo, R.; Züttel, A. *Mol. Phys.* **2009**, *107*, 1831–1842.
(26) Plane-Wave Self-Consistent Field: PWscf, Quantum-Espresso, 2009. http://www.pwscf.org.
(27) Refson, K.; Clark, S.; Tulip, P. *Phys. Rev. B* **2006**, *73*, 155114.
(28) Johnston, H. L.; Hallett, N. C. *J. Am. Chem. Soc.* **1953**, *75*, 1467–1468.
(29) Stockmayer, W. H.; Stephenson, C. C. *J. Chem. Phys.* **1953**, *21*, 1311–1312.
(30) Abrahams, S. C.; Kalnajs, J. *J. Chem. Phys.* **1954**, *22*, 434–436.
(31) Davis, R.; Kennard, C. *J. Solid State Chem.* **1985**, *59*, 393–396.
(32) Allis, D. G.; Hudson, B. S. *Chem. Phys. Lett.* **2004**, *385*, 166–172.
(33) Filinchuk, Y.; Hagemann, H. *Eur. J. Inorg. Chem.* **2008**, *2008*, 3127–3133.
(34) Caputo, R.; Tekin, A.; Sikora, W.; Züttel, A. *Chem. Phys. Lett.* **2009**, *480*, 203–209.
(35) Dergazarian, T. E. *JANAF Interim Thermochemical Tables*; Technical Report, USAEC Report; U.S. Atomic Energy Commission: Washington, DC, 1961.
(36) Sterlyadkina, Z. K.; Kryukova, O. N.; Mikheeva, V. *Russ. J. Inorg. Chem.* **1965**, *10*, 316–318.
(37) Albert, B.; Hofmann, K. *Z. Anorg. Allg. Chem.* **1999**, *625*, 709–713.
(38) Naslin, R.; Kasper, J. *J. Solid State Chem.* **1970**, *1*, 150–151.
(39) Albert, B.; Hofmann, K.; Fild, C.; Eckert, H.; Schleifer, M.; Gruehn, R. *Chem.—Eur. J.* **2000**, *6*, 2531–2536.